Dear Author,

Please correct your galley proofs carefully and return them no more than four days after the page proofs have been received.

Please limit corrections to errors already in the text; cost incurred for any further changes or additions will be charged to the author, unless such changes have been agreed upon by the editor.

The editors reserve the right to publish your article without your corrections if the proofs do not arrive in time.

Note that the author is liable for damages arising from incorrect statements, including misprints.

Please note any queries that require your attention. These are indicated with a Q in the PDF and a question at the end of the document.

Reprints may be ordered by filling out the accompanying form.

Return the reprint order form by fax or by e-mail with the corrected proofs, to Wiley-VCH : **afm@wiley.com**

To avoid commonly occurring errors, **please ensure that the following important items are correct** in your proofs (please note that once your article is published online, no further corrections can be made):

- **Names** of all authors present and spelled correctly

- **Titles** of authors correct (Prof. or Dr. only: please note, Prof. Dr. is not used in the journals)

- **Addresses** and **postcodes** correct

- **E-mail address** of corresponding author correct (current email address)

- **Funding bodies** included and grant numbers accurate

- **Title** of article OK

- All **figures** included

- **Equations** correct (symbols and sub/superscripts)

Corrections should be made directly in the PDF file using the PDF annotation tools. If you have questions about this, please contact the editorial office. The corrected PDF and any accompanying files should be uploaded to the journal's Editorial Manager site.

| Query No.	Description	Remarks
Q-license	Please note that the article can only be published once an appropriate license agreement has been signed. The responsible corresponding author will have received an e-mail invitation to register/log in and sign a license agreement in Wiley Author Services (https://authorservices.wiley.com). The costs of publishing this manuscript OnlineOpen might be covered by one of Wiley's national agreements. To find out more please visit, https://authorservices.wiley.com/authorresources/Journal-Authors/open-access/affiliation-policies-payments/index.html. Eligibility for fee coverage is determined by the affiliation of the responsible corresponding author.	
Q1	Please confirm that forenames/given names (blue) and surnames/family names (vermilion) have been identified correctly.	
Q2	Please provide the highest academic title (either Dr. or Prof.) for all authors, where applicable.	
Q3	Please define all acronyms at their first appearance in the abstract, text and table of contents, respectively. Only expanded forms are allowed if the elements are cited only once in the article.	
Q4	Please shorten the abstract to a maximum of 200 words. All abbreviations should be defined in their first instances.	
Q5	Please check the sentence 'To prepare the GNE ink were employed a solvent exchange method:...' for clarity.	
Q6	Please provide Table 2.	
Q7	Please check whether setting the sentence 'The GCE ink was used to fabricate the final electrodes to be used in the touch sensor prototype.' as table footnote is correct.	
Q8	Please check all equations have been correctly typeset.	
Q9	Please check the page number provided in ref. [9].	
Q10	Refs. 17 and 59 were identical hence ref. 59 has been deleted from the ref. list. Refs. have been renumbered both in the text and ref. list. Please verify.	
Q11	Please check ref. [21] for correctness.	
Q12	Please provide volume number for ref. [30].	
Q13	Please provide volume number for ref. [61].	
Q14	Please check the details provided in ref. [65]. Also provide the volume number.	

Please confirm that Funding Information has been identified correctly.

Please confirm that the funding sponsor list below was correctly extracted from your article: that it includes all funders and that the text has been matched to the correct FundRef Registry organization names. If a name was not found in the FundRef registry, it may not be the canonical name form, it may be a program name rather than an organization name, or it may be an organization not yet included in FundRef Registry. If you know of another name form or a parent organization name for a "not found" item on this list below, please share that information.

FundRef Name	FundRef Organization Name
GNESIS	
GEMIS "Graphene-enhanced Electro-Magnetic Interference Shielding"	
COMPETE 2020 "Operational Programme for Competitiveness and Internationalization and FCT" Science and Technology Foundation	
European Regional Development Fund	European Regional Development Fund
LAETA	
Fundação para a Ciência e a Tecnologia	Fundação para a Ciência e a Tecnologia

RESEARCH ARTICLES

S. Tkachev, M. Monteiro, J. Santos,
E. Placidi, M. B. Hassine, P. Marques,
P. Ferreira, P. Alpuim,*
A. Capasso*.............................. 2103287

Environmentally-Friendly Graphene Inks for Touch Screen Sensors

Liquid Phase Exfoliation
+
Spray Coating

Graphene Touch Sensor
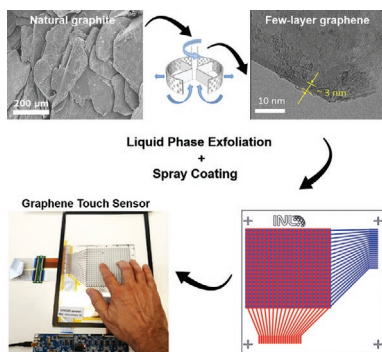
An efficient, inexpensive, and green strategy to produce graphene dispersions by liquid-phase exfoliation with high concentration is proposed. By a combination of shear mixing and tip sonication techniques in cyrene solvent, a graphene-based ink is made and spray-coated to fabricate a touch screen sensor prototype with a high signal-to-noise ratio (14 dB) and multi-touch functionality.

Environmentally-Friendly Graphene Inks for Touch Screen Sensors

Sergey Tkachev, Miguel Monteiro, João Santos, Ernesto Placidi, Mohamed Ben Hassine, Pedro Marques, Paulo Ferreira, Pedro Alpuim,* and Andrea Capasso*

Graphene-based materials have attracted significant attention in many technological fields, but scaling up graphene-based technologies still faces substantial challenges. High-throughput top-down methods generally require hazardous, toxic, and high-boiling-point solvents. Here, an efficient and inexpensive strategy is proposed to produce graphene dispersions by liquid-phase exfoliation (LPE) through a combination of shear-mixing (SM) and tip sonication (TS) techniques, yielding highly concentrated graphene inks compatible with spray coating. The quality of graphene flakes (e.g., lateral size and thickness) and their concentration in the dispersions are discussed and compared using different spectroscopic and microscopy techniques. Several approaches (individual SM and TS, and their combination) are tested in three solvents (N-methyl-2-pyrrolidone, dimethylformamide, and cyrene). Interestingly, the combination of SM and TS in cyrene yields high-quality graphene dispersions, overcoming the environmental issues linked to the other two solvents. Starting for the cyrene dispersion, a graphene-based ink is prepared to spray-coat flexible electrodes and assemble a touch screen prototype. The electrodes feature a low sheet resistance (290 Ω $\square^{-1}$) and high optical transmittance (78%), which provide the prototype with a high signal-to-noise ratio (14 dB) and multi-touch functionality (up to four simultaneous touches). These results illustrate a potential pathway toward the integration of LPE-graphene in commercial flexible electronics.

1. Introduction

Graphene, the archetypal 2D material, is a single layer of covalently bonded carbon atoms arranged in a honeycomb lattice with a thickness of 0.34 nm.[1] Since its isolation and study in 2004, graphene has become a pivotal subject of research due to many extraordinary properties, such as strength (between 100–300 times stronger than steel), lightweight, flexibility, transparency, high electrical and thermal conductivity.[2–4] With these motivations, graphene-based materials (GBM) has been heralded to impact a broad range of technological fields, such as electronics,[5] optoelectronics,[6] energy storage,[7] medicine,[8–10] and environmental safety.[3] GBMs could replace several well-established materials in many areas,[2,11–14] particularly in composites,[15] energy storage devices,[16] and flexible electronics.[17,18] In six years (from 2009 to 2015), GBMs' production increased from 14 tons to 120 tons, with production reaching 1800 tons at the end of 2020.[14,19,20] The global graphene market size was valued at $87.5 million in 2019 and is projected to reach $876.8 million by 2027, growing at a CAGR% of 40.2% from 2020 to 2027.[21] To date, graphene-based applications include organic light-emitting diodes, field-effect transistors, flexible and wearable devices,[11,22–24] photonic devices, electrodes for batteries, printed thin-film transistors, photodetectors, photovoltaic cells, sensors, and touch sensors.[22,25,26] Despite these advances, bringing a new material to the market is usually a challenging task. The innovation rooted in new materials is a challenging, long, and expensive pursuit, often unsuccessful since it requires the integration

Dr. S. Tkachev, M. Monteiro, J. Santos, Dr. M. B. Hassine,
Prof. P. Ferreira, Prof. P. Alpuim, Dr. A. Capasso
International Iberian Nanotechnology Laboratory (INL)
Braga 4715-330, Portugal
E-mail: pedro.alpuim.us@inl.int; andrea.capasso@inl.int
Dr. E. Placidi
Dipartimento di Fisica
Università di Roma La Sapienza
Roma 00185, Italy
P. Marques
Displax S.A.
Rua Soldado Manuel Pinheiro Magalhães, 68, Braga 4715-167, Portugal

Prof. P. Ferreira
Mechanical Engineering Department and IDMEC
Instituto Superior Técnico
University of Lisbon
Av. Rovisco Pais, Lisbo 1049-001, Portugal
Prof. P. Ferreira
Materials Science and Engineering Program
The University of Texas at Austin
Austin, TX 78712, USA
Prof. P. Alpuim
Departamento de Física
Universidade do Minho
Braga 4710-057, Portugal

**ADVANCED
SCIENCE NEWS**

www.advancedsciencenews.com

**ADVANCED
FUNCTIONAL
MATERIALS**

www.afm-journal.de

of the new materials in existent production lines and technology.[14] In the case of GBMs, several technological challenges have delayed mass production and the development of devices for the consumer market. However, many graphene synthesis techniques are currently available,[3,27,28] and some of those are compatible with an industrial setting. In this context, one of the most effective methods is liquid-phase exfoliation (LPE), which was initially reported in 1989 for MoS_2 and WSe_2.[29,30] For graphene, LPE was first demonstrated in 2008, opening the way to an intense research effort.[31] Since then, LPE has attracted considerable attention as a cost-effective and up-scalable method for the production of liquid dispersions of defect-free graphene flakes, which in turn may enable the fabrication of large-area, flexible, transparent, and printable electronics.[32,33]

In general, LPE refers to a group of techniques able to exfoliate a bulk van der Waals solid into its corresponding isolated layers by applying energy to disrupt the weak inter-layer bonds in a liquid medium.[33,34] LPE techniques can be classified into electro-chemical and physical exfoliation. Physical exfoliation encompasses processes such as ultrasonic exfoliation[31] and several shear exfoliation approaches,[35] which can be realized by high shear mixing, wet ball milling,[36] micro-fluidization,[37] homogenization,[38] and wet jet milling.[39] Physical exfoliation techniques can be performed using various solvents such as water, surfactants, organic solvents, ionic liquids, oils, and salts.[33,40,41] The choice of an appropriate solvent hinges on several factors that are either inherent to the solvent's fluidic properties or related to the processing method, such as potential solvent toxicity, too high a boiling point, or limited substrate compatibility. Research on conductive graphene-based dispersions has been progressing steadily. Paton et al. recently demonstrated a scalable production method to obtain large quantities of dispersed graphene nanosheets by shear-mixing. The group reported exfoliation with shear rates of $\approx 10^{-4}$ s^{-1}, achievable by simple setups and compatible with other layered materials, such as MoS_2 and BN.[38] Arao and Kubouchi proposed high-power probe-sonication with optimized processing conditions to obtain a few-layer graphene production rate over 1 g h^{-1} in N-methyl-2-pyrrolidone (NMP), ideal for mass production at a low cost.[42] Durge et al. obtained ≈ 1.2 g L^{-1} of graphene nanosheets after a 120-min probe sonication in dimethylformamide (DMF)—ten times higher a concentration than that obtained by bath sonication in the same solvent.[43] To replace these two dipolar aprotic solvents (NMP and DMF), abundantly used in this field but toxic and presenting severe health risks, Salavagione et al. conducted a systematic study on alternative solvents. The authors concluded that the green solvent cyrene had excellent properties, namely an optimum solvent polarity and a high viscosity.[32] Graphene dispersions in cyrene were an order of magnitude more concentrated than those achieved in NMP. Pan et al. have also used cyrene as LPE solvent to produce graphene inks compatible with screen-printing technology, fabricating devices with high electrical conductivity such as antennas.[44]

Touch screen sensors are an ubiquitous part of modern electronic technology, granting users a direct way to interact with devices. Nowadays, several touch surfaces can be found in consumer electronics, like drawing tablets,[45] keyboards with touch surfaces,[46] and other touch-sensitive user interfaces.[47]

In display technology, the sensors are usually placed in front or embedded in the device's display, allowing direct interaction with the screen's information. Capacitive sensors are one of the most commonly used touch sensor types due to their durability, performance, high sensitivity, and multitouch capabilities. In capacitive sensing, the touch location is determined by capacitance variation across the sensor. Electrode arrays are typically arranged in two layers (isolated by a dielectric), one for rows and the other columns (X and Y axes), used as driving (or transmitter) and sensing (or receiver) electrodes, respectively. For transparent touch sensors, transparent conductive oxides (TCO) such as indium tin oxide (ITO) or aluminum-doped zinc oxide (AZO) are widely used as electrodes.[48] In 2020, a flexible capacitive touch sensor based on ITO could reach a sheet resistance of ≈ 6 Ω □$^{-1}$ with an optical transmittance of $\approx 91\%$ (at 550 nm).[49] Although these oxides can grant high-performance, they are quite expensive and not environmentally friendly (e.g., they are not easily recyclable, and ITO in particular relies on a critical material, In).[25,50] These characteristics, combined with a general brittleness, make ITO and AZO unsuitable for application in stretchable and conformal devices, such as wearable electronics and bendable displays. As such, these limitations have motivated an increased research effort toward alternative solutions, based on Ag-based materials[51,52] and GBM.[25] A wide range of GBMs have been proposed. Kang et al. developed a flexible touch sensor based on tri-layer, trifluoromethanesulfonic acid (TSFA)-doped, CVD-grown graphene electrodes with a sheet resistance of ≈ 320 Ω □$^{-1}$ and an optical transmittance of $\approx 85\%$.[25] Despite graphene-based sensors have yet to achieve the performance reached by TCO-based ones, the flexibility granted by the GBM production techniques allows for several routes toward significant improvements. Prospective techniques to produce and process technology over large scales should focus not only on performance achievements but also on cost-related factors and sustainability.

Our work explores a novel and highly effective LPE approach to produce graphene that consists of high-speed shear mixing (SM) and tip sonication (TS). Our approach simultaneously improves the production yield (in terms of concentration) and the exfoliated flakes' quality, that is, granting thinner flakes with a specific lateral size. We study the performance of a combination of SM+TS processes for exfoliating graphite in NMP, comparing with the results obtained by individual TS and SM processes. We estimated the yield (by measuring the concentration) and the graphene flake quality (i.e., thickness, lateral size, and defect level) granted by each process. Building on this knowledge, we explored and optimized the exfoliation by a combination of SM+TS processes in cyrene, a biocompatible solvent: we were able to produce highly concentrated dispersions (up to 3.70 g L^{-1}) of graphene flakes with average lateral size of ≈ 200 nm. Our LPE approach in cyrene is an up-scalable, cost-effective, and environmentally friendly route toward the industrial adoption of graphene in various fields, such as electronics. To demonstrate this, we further processed the cyrene dispersions into functional graphene inks by a solvent exchange technique, in order to re-disperse the graphene flakes in low-boiling-point ethanol and make them compatible with spray coating deposition. With these graphene-based inks, we designed and fabricated transparent conductive electrodes

suitable for a wide range of electronic devices. We explored these electrodes in an industrial framework by fabricating a prototype of a semi-transparent projected capacitive field touch screen sensor. The graphene-based electrodes had suitable characteristics to grant the graphene-based touch sensor with a high signal-to-noise ratio (SNR = 14 dB) and multi-touch functionality, while keeping a high optical transmittance (≈78%). Remarkably, the sensor featured multi-touch functionality (up to four simultaneous touches). Overall, our experimental approach provides a solution to the concerning issues related to standard LPE-graphene production, demonstrating a viable and effective route to fabricate graphene-based technology in an industrial framework.

2. Experimental Section

2.1. Materials

Natural graphite 332461 (NG), NMP anhydrous (99.5% purity), DMF (99.8%), cyrene (98%), silver nitrate ($AgNO_3$, 99.0%), ethanol (99.0%), ethylene glycol (EG, 99.0 %), polyvinylpyrrolidone (PVP, M_W = 40 000) were purchased from Sigma-Aldrich and used without further purification.

2.2. Liquid-Phase Exfoliation and Graphene Dispersion Preparation

For the LPE processing of NG, three different solvents were used: NMP, DMF, and cyrene. 30 g of NG powder was dispersed in 600 mL of solvent. Three different LPE methodologies were used: A) TS (10 h); B) SM (10 h); and C) SM (10 h) and TS (10 h). The TS process was performed using an ultrasonic disruptor (Branson Digital Sonifier SFX 550, 0.55 kW of power at 20 kHz frequency for high-volume processing, 1/2″ disruptor horn with 1/2″ extension type tip). The SM process was carried out using a high-shear laboratory mixer Silverson L5M (standard mixing assembly with an emulsor screen and an axial flow head). In each case, the SM process (10 h) consisted of two steps: mixing with emulsor screen (8 h, 7500 rpm) and mixing with emulsor screen and axial flow head (2 h, 5000 rpm). An ultracentrifugation stage was carried out after each exfoliation procedure to remove un-exfoliated bulk graphite and thicker flakes: 3000 rpm for 40 min for dispersions in NMP and DMF; 9000 rpm for 40 min for dispersion in cyrene (due to the higher viscosity of the solvent). After ultracentrifugation, the supernatant was extracted and collected in a bottle.

2.3. Ink Characterization

2.3.1. Thermogravimetric Analysis

Thermogravimetric analysis (TGA) was performed to determine the concentration of graphene flakes in NMP, DMF, and cyrene dispersions. A known volume of the graphene dispersion was previously sonicated for 5 min to guarantee that the particles were well dispersed. A drop of the dispersion was cast in a petri dish of known weight, then left to dry in an oven for 24 h (right below the boiling point temperature of each solvent). Finally, the weight was measured.

2.3.2. Raman Spectroscopy

Dispersion samples were diluted with isopropyl alcohol to yield a pale colloidal solution (0.005 g L^{-1}). 20 µL were then drop-cast into a preheated (120 °C) 1×1 cm SiO_2 (300 nm) substrate and left to dry 2 min and rinsed with 5 mL of isopropyl alcohol (IPA). Raman spectra were collected with an Alpha300R Confocal Raman Microscope (WITec) using a 532 nm wavelength laser (2.33 eV) focused with a 100× objective lens (Zeiss) and an incident power of 1.2 mW. An acquisition time of 2 s was used, together with a 600 g mm^{-1} grating. More than 30 points were acquired for each sample. Lorentzian functions were used to fit the peaks in the spectra.

2.3.3. Transmission Electron Microscopy

The flakes from each dispersion were characterized by transmission electron microscopy (TEM) using a probe-corrected FEI Titan 80–200 ChemiSTEM microscope operated at 80 kV. For sample preparation, the flakes were dispersed in ethanol with ultrasonication, drop-cast onto a holey carbon-coated 300 mesh Cu grid, and dried by a lamp. The bright field TEM images were collected using a CCD Gatan UltraScan camera. The lateral sizes of the flakes were measured as the longest distance of the flakes obtained by the TEM images.

2.3.4. Atomic Force Microscopy

The graphene flakes were analyzed by atomic force microscopy (AFM) to measure size and thickness. Samples were prepared by diluting the dispersions in isopropyl alcohol (0.005 g L^{-1}). 20 µL were then pipetted on a preheated (120 °C) 1×1 cm SiO_2 (300 nm) substrate, left to dry for 2 min, and finally rinsed with 5 mL of IPA. AFM topographies were acquired with a Veeco Multimode (Nanoscope IIIa) in AM mode (tapping mode), employing Si tips with a nominal radius of curvature of ≈7 nm. The image analysis was performed with Gwyddion,[53] optimizing the graphene foils selection with a grain analysis package. Measurements were taken from over 200 individual flakes for each sample to get a reliable statistic of the lateral size distribution.

2.3.5. X-Ray Photoelectron Spectroscopy

X-ray photoelectron spectroscopy (XPS) spectra were acquired with a hemispherical electron energy analyzer (PHOIBOS 150—SPECS). XPS characterization was performed in ultrahigh vacuum (base pressure of 10^{-8} Torr) with a twin Al anode X-ray source XR50 (SPECS) operated at 12 keV. 100 W power was used to excite the photoelectron spectra. The XPS spectra were acquired in the fixed analyzer transmission mode with pass energies of 20 and 100 eV (just for survey spectra) and

0.1 eV energy step for detecting elemental spectral lines with high resolution. The calibration of the binding energy was performed considering as reference the graphitic signal at 284.4 eV. The XPS spectra were peak-fitted using KolXPD data processing software. The quantification used sensitivity factors provided by the elemental library of the Avantage software.[54] The background was fitted with a Shirley curve. The sp^2 peak was fitted with a convolution of a Doniach-Sunjic curve and a Voigtian curve. The asymmetry parameter was determined by the cleanest spectrum (cyrene-post) and kept fixed for all the other fits. The Lorentzian width was constant for all the components, while the Gaussian widths free to evolve. The chemical shifts of all components relative to the sp^2 were kept fixed for all the fittings.

2.4. Fabrication and Characterization of the Touch Screen

2.4.1. Materials

The SM+TS dispersions in NMP and cyrene were further processed to produce two graphene-based inks suitable for spray-coating—which were named "GNE" ink and "GCE" ink, respectively. To prepare the GNE ink were employed a solvent exchange method: first, 32 mL of the dispersion in NMP was filtered (via a PFET filter, with 0.2 µm pore size) using vacuum filtration.[55] The flakes collected in the filter were then recovered by ultrasonication in 100 mL of ethanol (10 min, 37 kHz frequency, Elmasonic P by Elma), completing the so-called solvent exchange method. After the sonication, 1 mL of PEDOT:PSS solution (1 wt%) was added to the 100 mL ethanol dispersion, followed by 5 min sonication in a water bath sonication and 15 min stirring at room temperature (the minimal amount of PEDOT:PSS was meant to improve the adhesion among flakes and the substrate, reducing the sheet resistance). To prepare the GCE ink, 14 mL of the dispersion in cyrene was filtered (via a PFET filter, with 0.2 µm pore size) using vacuum filtration. The same steps as for the GNE ink were thus followed.

Both GNE and GCE inks were designed to have a final graphene flake concentration of 0.5 mg mL^{-1}. Ag nanoparticle (NP) inks were prepared by reducing AgNO$_3$ in an ethylene glycol (EG) solution with PVP. 1 g of PVP and 0.015 g NaOH were dissolved in 100 mL EG in an oil bath at 60 °C with continuous magnetic stirring for 1 h. A solution of 1.5 g of AgNO$_3$ in 10 mL of deionized water was added drop by drop, keeping temperature constant. When the mixture turned to light yellow-brown, the rest of the AgNO$_3$ solution was injected slowly for 1 min while stirring. The solution was further stirred for two hours at 60 °C. The mixture was then heated up to different temperatures step by step while stirring: 80 °C (2 h), 100 °C (2 h), 120 °C (2 h). Then 300 mL of acetone was added to the mixtures to initiate the NPs sedimentation, removing the PVP excess. The as-produced Ag NP colloid was centrifuged at 9000 rpm for 10 min, washed again by acetone, and dried gently under N$_2$ flow. The resulting Ag NPs (≈33 nm, Figure S1, Supporting Information) were re-dispersed in 10 mL of ethanol to make the Ag ink used to fabricate the conductive pads.

2.4.2. Electrode Fabrication and Measurements

20 mL of each GNE and GCE ink were used to spray-coat a rectangular electrode (2 × 20 cm^2) on a PET substrate using an airbrush (Richpen 112B, Japan) with N$_2$ carrier gas (nozzle diameter ≈ 0.2 mm, airbrush kept perpendicularly at 8 cm from the substrate, flow rate ≈ 5 mL N$_2$ min^{-1}, pressure 1 bar). Profilometry (KLA—Tencor P-16 Surface Profiler) was used to measure and control the electrode thickness. The sheet resistance was measured with a 4-point probe station (Jandel, RM3000) with a parameter analyzer (Keithley, 4200C). The optical transmittance spectra (300–800 nm range, ten spectra collected and averaged for each sample) were acquired with a PerkinElmer LAMBDA 950 UV–vis–NIR spectrometer.

2.4.3. Touch Screen Fabrication

GCE was used to fabricate a semi-transparent projected capacitive (pro-cap) touch sensor prototype, working in mutual capacitance mode. Custom vinyl hard masks were designed and cut using a Silhouette Cameo 2 to create the pattern for both the graphene channel electrodes and Ag connection pads on a 17 cm × 17 cm PET substrate. Two sheets with 20 graphene electrodes for columns (top panel) and 20 for rows (bottom panel) form the sensor area into a diamond-shaped mesh of nodes (**Figure 1**). The graphene ink was sprayed onto the top and bottom panels (same conditions described in Section 2.4.2). The Ag inks were spray-coated on the PET/graphene substrates through a custom vinyl mask (designed to protect the previously fabricated graphene electrodes—i.e., the sensing element) using an airbrush (nozzle diameter ≈ 0.2 mm, airbrush
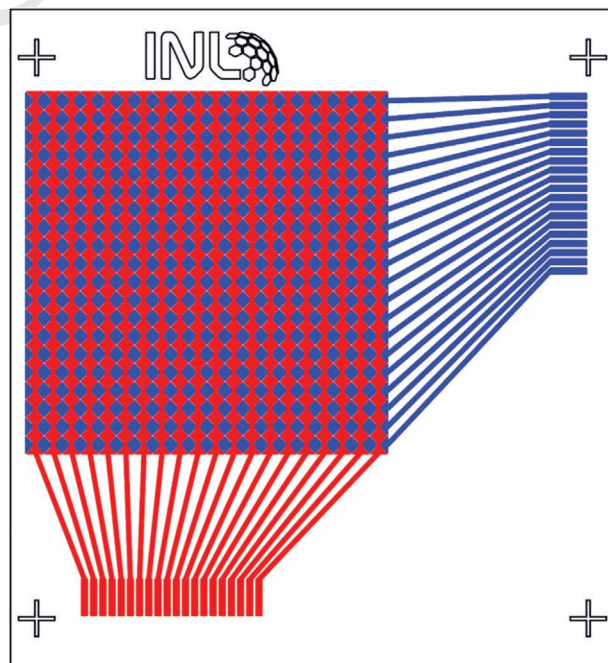

Figure 1. The developed design of a projected capacitive (pro-cap) touch screen. After characterization (Section 2.4.4), the top and bottom panels were laminated together with a dielectric spacer in between.

kept perpendicularly at 8 cm from the substrate) with N_2 (flow rate ≈ 5 mL N_2 min^{-1}, pressure 1 bar).

After coating, the vinyl masks were carefully peeled off the PET substrate, let dry at room temperature for 10 min, and then at 100 °C for 10 min. The Ag conductive pads connected to the graphene electrodes' edges in the top and bottom panels (red and blue linear connections in Figure 1) served as external contacts to the control electronics.

2.4.4. Electrical and Optical Characterization of the Touch Sensor

Electrode resistance measurements were performed using an ohmmeter connected to both ends of each electrode. This configuration allowed to check the electrical continuity and potential short-circuits between electrodes. The sensor transmittance was measured with a Linshang Technology LS162 transmission meter (accuracy higher than ±2%, 99.9% ultraviolet rejection rate, and infrared rejection rate > 85%).

The sensor was electrically scanned using an electronic controller. The controller monitored the capacitive charge on each crossing (or node) between the vertical and horizontal electrodes. The industry referred to this technique as mutual capacitance scanning. The electronic controller applied an AC current into each horizontal electrode (using an 18 V voltage amplitude). The capacitive charges were received on the vertical electrodes, measured differentially to remove any common-mode electrical noise, and converted to digital information. If the sensor was touched, the corresponding node had a different charge value. Afterward, the controller's firmware compared the charge values and, through specialized algorithm techniques, identified the touched positions, and reported them via USB HID protocol to the final host system (see also the discussion relating to Figure S4, Supporting Information).The sensor's optical transmittance was measured in the visible range (380–760 nm) using a portable Linshang Technology LS162 transmission meter (Supporting Information).

3. Results and Discussion

3.1. Characterization of the Graphene Dispersions

We developed an optimized LPE approach to produce graphene dispersions with flake size distribution compatible with spray coating by combining SM and TS techniques. The characteristics of the exfoliated graphene flakes in the dispersions depend significantly on the solvents' surface energy. To facilitate the exfoliation and obtain a stable dispersion of atomically thick graphene flakes, the solvent's surface tension (γ) should approximate graphite's surface energy (ς ≈ 55 mJ m^{-2}).[31,35,56] For this reason, *N*-methyl-2-pyrrolidone (NMP, γ ≈ 68.2 mJ m^{-2}) and *N,N*-dimethylformamide (DMF, γ ≈ 65 mJ m^{-2}) are commonly used solvents since they allow to effectively exfoliate and suspend the graphene flakes without any stabilization agents.[32] These solvents, however, require a post-process annealing (at temperatures above 150 °C) to remove residues after the deposition of the graphene flakes.[30,57] In addition to toxicity issues, the need for post-processing makes these solvents non-ideal

choices for production and commercialization. For the LPE of graphite, green, and low-boiling-point solvents (such as alcohols, water, or mixtures of both) do not typically provide high stability over time; besides, the amount of graphene flakes obtained in dispersion is consistently lower than obtained with high-boiling-point solvents.[58] For these reasons, stable dispersions in low-boiling-point solvents generally require the addition of stabilizing agents, such as surfactants or polymers. These additives, however, have been reported to produce undesirable effects, such as reduced optical transmittance and electrical conductivity in the deposited films, which consequently require annealing treatments at high temperatures (>350 °C) or chemical post-processing (Table S1, Supporting Information).[17]

We explored a combination of SM and TS processes to i) maximize the exfoliation yield in different solvents and ii) understand the effect on the flake size. The TGA analysis of the NMP dispersions showed that SM provided a higher exfoliation yield than TS does (0.44 and 0.29 mg mL^{-1}, respectively). Remarkably, SM and TS's combination granted the highest concentration among all exfoliation methods (1.6 mg mL^{-1}). We characterized the graphene flakes produced by the different exfoliation approaches. Raman spectroscopy is a nondestructive technique that characterizes the graphene material's thickness, lateral size, and electronic doping. The Raman spectrum presents three prominent bands at 1350 cm^{-1} (D band), 1580 cm^{-1} (G band), and 2700 cm^{-1} (2D band, also called G′).[59–61] The G band is due to the in-plane vibrational mode involving the sp^2-hybridized carbon atoms in the graphene lattice, corresponding to the E_{2g} phonon at the Brillouin zone center.[61] The G band position is susceptible to the number of layers and can be used to estimate thickness: the peak position downshifts to ≈1581 cm^{-1} in few-layer graphene compared to ≈1587 cm^{-1} in monolayer graphene.[62] The G band position (Pos$_G$) and its width (FWHM$_G$) can infer the presence/level of defects in the flakes,[63] chemical doping,[59,64,65] or strain.[66] The D band arises from the breathing mode of sp^2 bonded carbon rings and requires the proximity of a defect for its activation by a double resonance process. The defects activating the D band can be either point defects in the basal plane or those due to unsaturated bonds in a flake's edges.[67] As such, I_D and the I_D/I_G ratio usually provide information on the average lateral size of the LPE graphene flakes: Smaller flakes have proportionally higher ratios of carbon atoms in the proximity of boundaries, contributing to the D band intensity.[61,68] The 2D band is the second order/overtone of the D band. It originates from two phonon lattice vibrational processes, but it is not necessarily activated by the proximity to a defect, unlike the D band. As a result, the 2D band is always prominent in the spectrum of crystalline monolayer graphene. The 2D band position (Pos$_{2D}$) in graphene is generally ≈2675 cm^{-1}, and flakes with more layers usually exhibit an upshift in position.[69,70] Pos$_{2D}$ and the I_{2D}/I_G ratio are commonly used to estimate the number of layers in graphene samples.[71] Additionally, the position of the 2D peak can be influenced by doping effects.[72] The position and shape of the 2D band can also provide information on graphene's thickness: A monolayer should consist of a single Lorentzian component, while multilayer graphene and graphite usually require multiple Lorentzian components to be fitted.[59,61,73] It should be noted that the 2D band is a resonant band with

**ADVANCED
SCIENCE NEWS**
www.advancedsciencenews.com

**ADVANCED
FUNCTIONAL
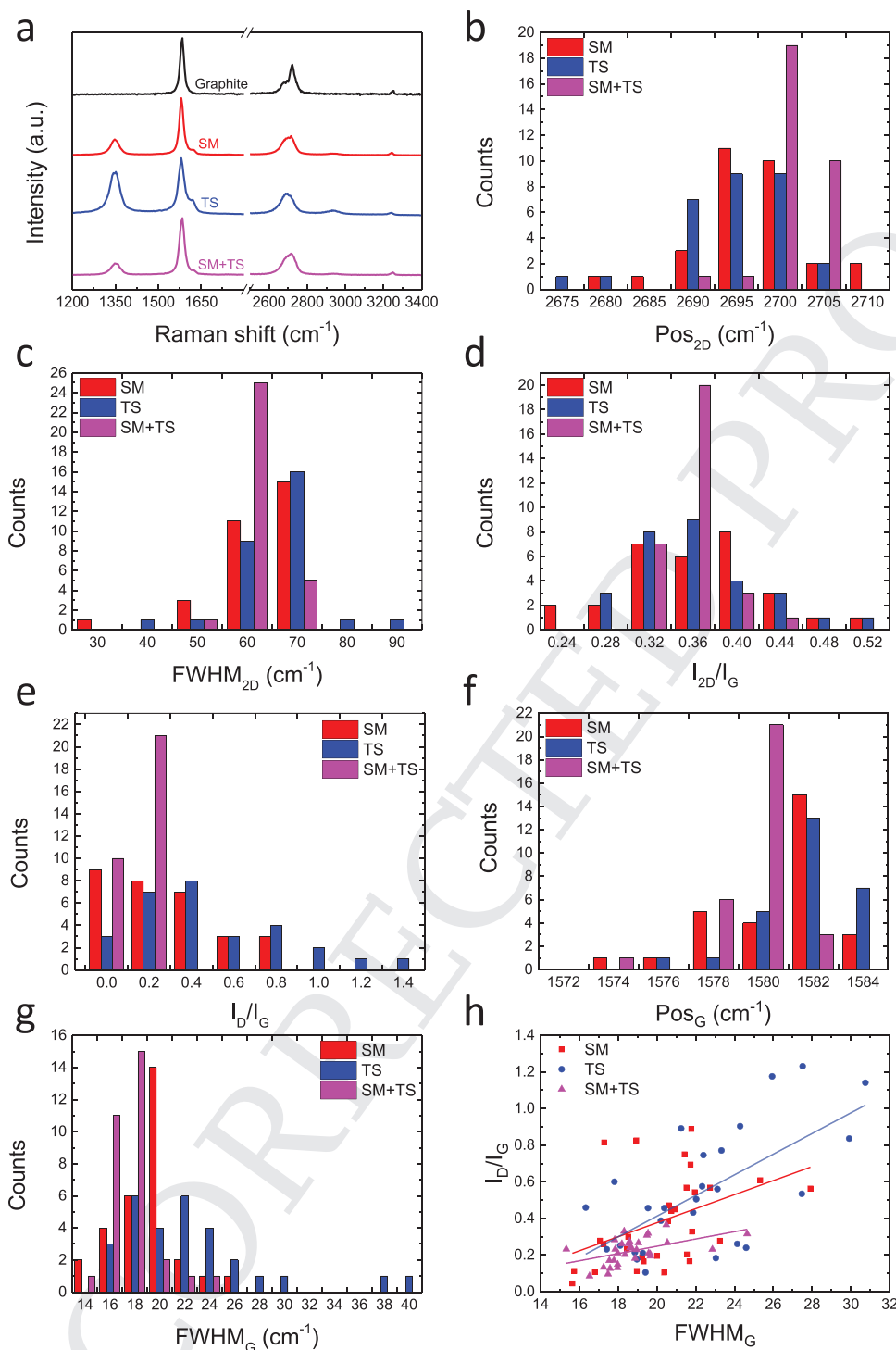MATERIALS**
www.afm-journal.de

Figure 2. a) Raman spectra representative of graphene flakes obtained by the different LPE processes in NMP (exfoliated from NG bulk material) to a bulk graphite sample; Distribution of b) Pos_{2D}, c) $FWHM_{2D}$, d) I_{2D}/I_G ratio, e) I_D/I_G ratio, f) Pos_G, g) $FWHM_G$, and h) I_D/I_G ratios as a function of $FWHM_G$.

dispersive behavior, that is, the band position is dependent on the laser excitation wavelength.[74]

Figure 2a compares the representative Raman spectra of graphene flakes obtained by the different LPE processes in NMP (exfoliated from NG bulk material) to a bulk graphite sample.

The three spectra corresponding to the three different processes show expected and similar features: The only apparent difference is a more intense D band for the TS sample. An accurate statistical analysis of the spectral features was performed by collecting multiple spectra on more than 30 flakes produced

by each of the three processes (see Experimental Section). We find that the 2D band position (Pos_{2D}) is peaked at ≈2695 cm^{-1} for SM and TS flakes, while it is consistently upshifted at ≈2700 cm^{-1} for SM+TS flakes (Figure 2b). The full width at half maximum of 2D ($FWHM_{2D}$) of the three sets is peaked at ≈70 cm^{-1} for SM and TS flakes and at ≈60 cm^{-1} for SM+TS flakes (Figure 2c), which would be the thinnest among the three.[73] The I_{2D}/I_G ratios are grouped predominantly between ≈0.32 and ≈0.40 (Figure 2d), with SM+TS flakes having the narrowest distribution. These spectral features indicate that all three processes produce few- to multilayer graphene flakes.[75] The SM+TS flakes (having the narrowest $FWHM_{2D}$ distribution) present the lowest variation in layer number.[73] The Raman spectra show significant D and D″ peaks intensity in all cases, with I_D/I_G ranging up to 0.8, 1.4, and 0.2 for SM, TS, SM+TS flakes, respectively (Figure 2e). In LPE samples, a high D band could be attributed to the edges of sub-micrometer flakes[76] rather than to a prevalence of structural defects within their basal plane. Indeed, if any defects are present in the graphene's basal plane, the G and D″ peaks become broader, merging into a single wideband,[77] which does not occur in these spectra. The Pos_G of the three sets of samples is peaked between 1580–1582 cm^{-1}, as expected for a few- to multilayer graphene. Here, the SM+TS flakes show the narrowest distribution once more, indicating the highest degree of control over the thickness distribution (Figure 2f). $FWHM_G$ is a measure of the number of defects; an increased $FWHM_G$ is a synonym with a higher defect density.[63] In Figure 2g, we observe that while SM and SM+TS flakes show comparable $FWHM_G$ values, TS flakes exhibit higher $FWHM_G$ values, which might be linked to a higher defect density induced by this technique. Plots of the I_D/I_G ratio versus $FWHM_G$ can provide further information. As mentioned, high I_D/I_G ratios suggest either a largely defected sample or small flake sizes.[78,67,79] When the I_D/I_G ratio and $FWHM_G$ are linearly correlated, the more defected samples also show the higher I_D/I_G ratios. In Figure 2h, there is no clear correlation between I_D/I_G and $FWHM_G$ for any of the samples exfoliated through the three techniques: The major contributor to the D band must come from the flakes "edges rather than from defects within the flakes" basal planes.[11] Therefore, the flakes produced by SM+TS, having the lowest I_D/I_G ratio range, should have the largest lateral size of the lot, followed by those produced by SM.[80]

Dispersions in DMF and cyrene were also prepared using the three different exfoliation approaches mentioned in Section 2.2. Similar concentration trends were observed for DMF and cyrene, as summarized in **Table 1**.

The graphene dispersions in DMF showed partial sedimentation after a one-month shelf-life test. Remarkably, the dispersions in cyrene showed the highest yield in all cases, with the SM+TS having a 3.70 mg mL^{-1} concentration. For this reason, and considering the large lateral size and narrow thickness distribution evidenced by the Raman analysis, the combination of SM+TS processes was selected for further investigation in the three solvents.

Figure 3a shows the representative Raman spectra of graphene flakes in NMP, DMF, cyrene. For DMF flakes, the Pos_{2D} peaks at ≈2705 cm^{-1} but is widely scattered, indicating poor thickness control. For NMP flakes, Pos_{2D} peaks at ≈2700 cm^{-1}, indicating thinner flakes than those exfoliated in cyrene, which peaks at ≈2705 cm^{-1}; both NMP and cyrene show a narrower distribution of Pos_{2D}, indicating a more controlled thickness distribution (Figure 3b). NMP and DMF flakes have an $FWHM_{2D}$ peaked at ≈65 cm^{-1}, while cyrene flakes have it at ≈60 cm^{-1} (in an overall lower range) (Figure 3c), which indicates that the latter are typically thinner. The I_{2D}/I_G ratios are grouped differently for the three sets of samples (Figure 3d). NMP flakes have the narrowest distribution with a marked peak at ≈0.36. DMF and cyrene flakes have overall broader distributions (between 0.24–0.40 and 0.24–0.48, respectively). NMP flakes thus seem to possess a narrow thickness distribution. Cyrene flakes have the broadest I_D/I_G ratio distribution, up to 0.50, indicating the occurrence of small lateral sizes (Figure 3e). Based on the Pos_G band position (Figure 3f), all solvents seem to yield few- to multilayer graphene. For cyrene flakes, the Pos_G range is the narrowest and peaked at the highest value (≈1582 cm^{-1}), indicating the smallest thickness of the lot.[62] In Figure 3g, we observe comparable $FWHM_G$ values for all samples, possibly indicating comparable residual chemical doping levels. As evidenced in Figure 2h, the lack of correlation between $FWHM_G$ and I_D/I_G suggests that I_D/I_G increments are due to the flakes' edges (Figure 3h). Addition Raman data, in line with those described above, can be found in Figure S2, Supporting Information.

TEM imaging revealed that the graphene flakes in NMP and cyrene had various different thicknesses in the multi-layer range. It also allowed to shed light on the lateral size of the flakes. **Figure 4** shows typical bright-field TEM images of flakes from NMP and cyrene dispersions. The graphene flakes show a flat morphology. They easily agglomerate on the TEM grid (to reduce their surface energy), making it difficult to locate individual monolayer regions. A careful examination of the edge of the flakes carried out by tilting the samples under the electron beam shows that the flakes exhibit few-layer thickness. Yet, the two solvents have a different effect on the thickness and lateral size of the flakes. The SM+TS process in cyrene seems to lead to smaller and thinner flakes than SM and SM+TS processes in NMP. By measuring 40 flakes using several TEM images from each sample, the average lateral size for both SM and SM+TS

Table 1. Concentration and stability of graphene dispersions prepared by exfoliating bulk NG. Three processes were tested by using three solvents (NMP, DMF, cyrene). The concentration is calculated by the TMG method. The stability is evaluated as a shelf-life after one month.

LPE process	Graphene dispersions in NMP		Graphene dispersions in DMF		Graphene dispersions in cyrene	
	Conc. [mg mL^{-1}]	Stability	Conc. [mg mL^{-1}]	Stability	Conc. [mg mL^{-1}]	Stability
TS	0.29	+	0.10	partial sedimentation	1.22	minimal sedimentation
SM	0.44	+	0.20	partial sedimentation	2.24	+
SM+TS	1.61	+	0.30	partial sedimentation	3.70	+

**ADVANCED
SCIENCE NEWS**

www.advancedsciencenews.com

**ADVANCED
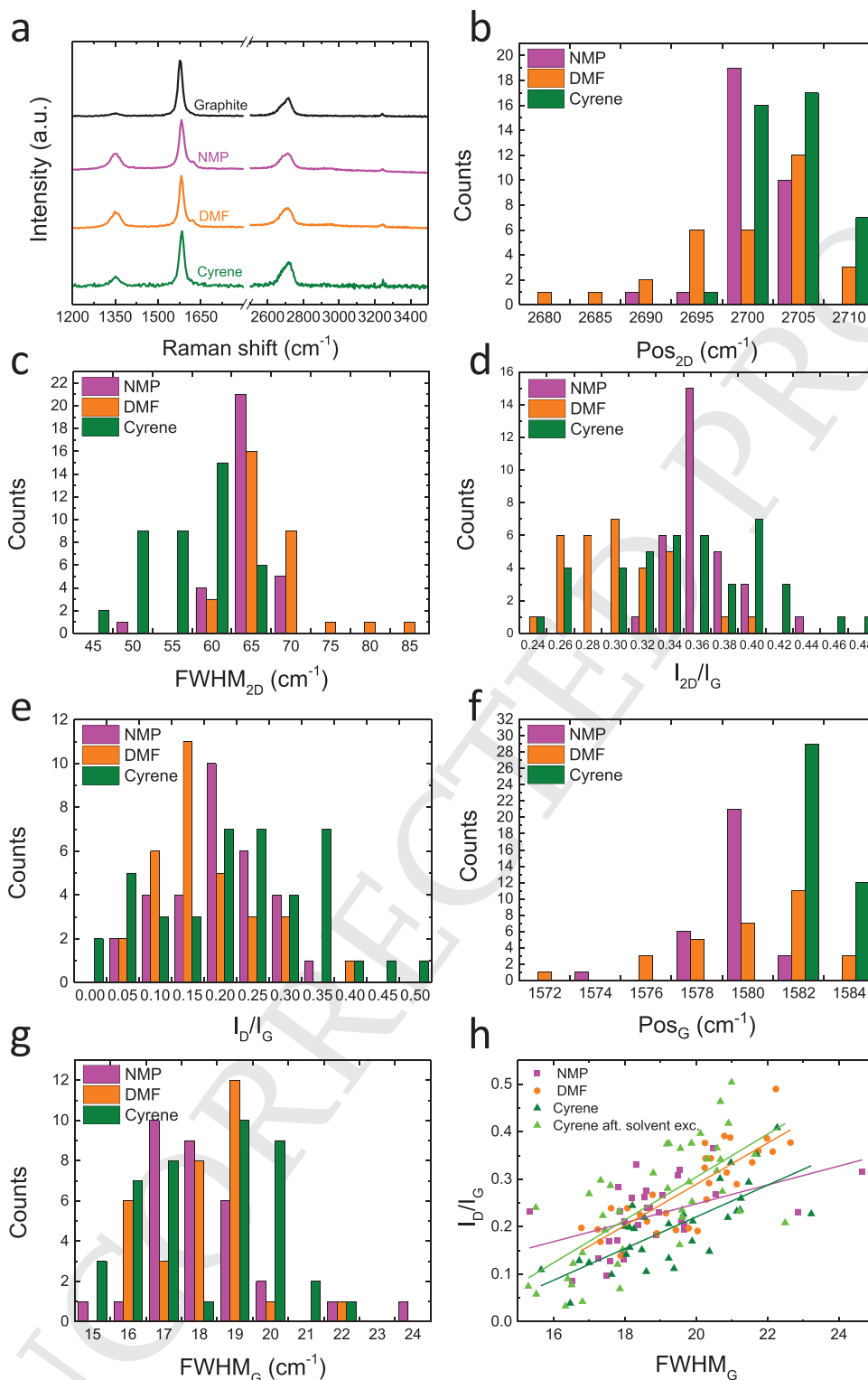FUNCTIONAL
MATERIALS**

www.afm-journal.de

Figure 3. Raman analysis of graphene flakes exfoliated in different solvents by using process SM+TS. a) Representative Raman spectra; Distribution of b) Pos_{2D}, c) $FWHM_{2D}$, d) I_{2D}/I_D ratio, e) I_D/I_G ratio, f) Pos_G, g) $FWHM_G$, and h) I_D/I_G ratios as a function of $FWHM_G$.

flakes in NMP appeared in the order of ≈500 nm; while with cyrene it was ≈100 nm for SM flakes and ≈200 nm for SM+TS flakes. It should be noted that such measurements might be overestimated due to the possible agglomeration of flakes on the TEM grids. Overall, the graphene flakes in NMP were consistently larger than those in cyrene.
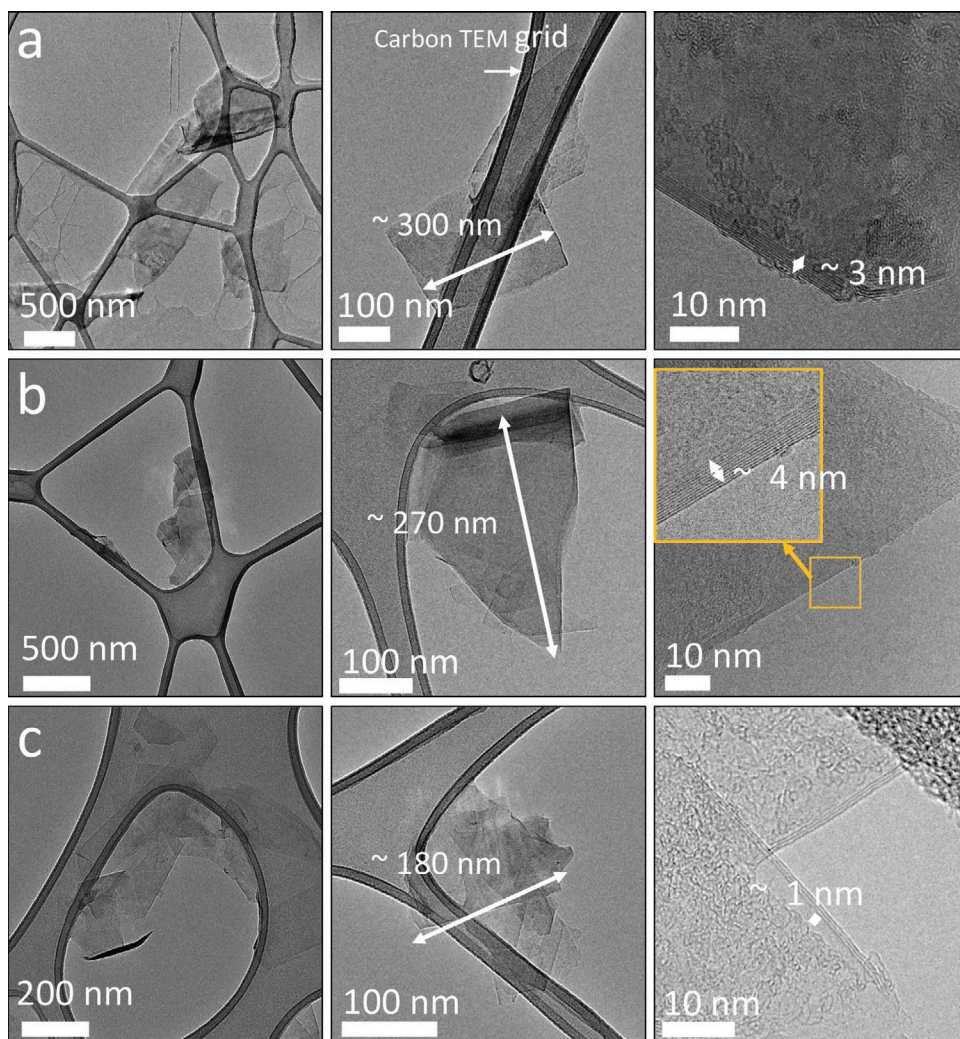
**ADVANCED
SCIENCE NEWS**
www.advancedsciencenews.com

**ADVANCED
FUNCTIONAL
MATERIALS**
www.afm-journal.de

Figure 4. Bright-field TEM images of the graphene flakes at different magnifications (increasing from left to right). a) Flakes were processed by SM in NMP, b) SM+TS in NMP, and c) SM+TS in cyrene. The white arrows in the second column highlight the average lateral size of several flakes. The yellow arrows in the third column indicate the flake thickness, as observed edge-on of the folded graphene.

The SM+TS flakes obtained in NMP and cyrene were also analyzed by AFM (**Figure 5**). The graphs in Figure 5 plot the frequency of flakes (counts) in lateral size.

The lateral size histograms follow a log-normal distribution, peaking at ≈75 nm and ≈125 nm for flakes produced in NMP and cyrene, respectively. The flake sizes shown in AFM are smaller than those estimated by TEM image analysis, most likely due to the aggregation of flakes on the TEM grids. Overall, the SM+TS processes produce graphene flakes with lateral size within 500–600 nm. The SM+TS graphene flakes

in NMP and cyrene were selected to prepare semi-transparent and electrically conductive inks suitable for spray coating deposition. A solvent exchange approach was used to re-disperse the flakes in ethanol (see the Experimental Section 2.4.1). An XPS analysis was performed to evaluate the chemical composition and bonding states of the graphene flakes from dispersions in NMP, cyrene, and ethanol (after solvent exchange from original cyrene). The XPS C1s spectra of the graphene flakes cast on Si are shown in **Figure 6**. The oxygen-containing functional group content of graphene flakes and residues
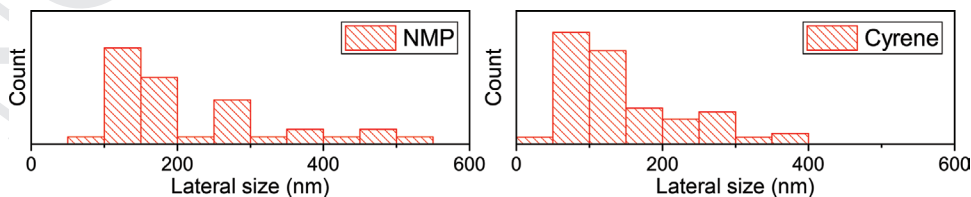

Figure 5. Histograms of lateral size obtained from the AFM analysis of graphene flakes produced by SM+TS in NMP (left) and cyrene (right) solvents.

ADVANCED
SCIENCE NEWS
www.advancedsciencenews.com

ADVANCED
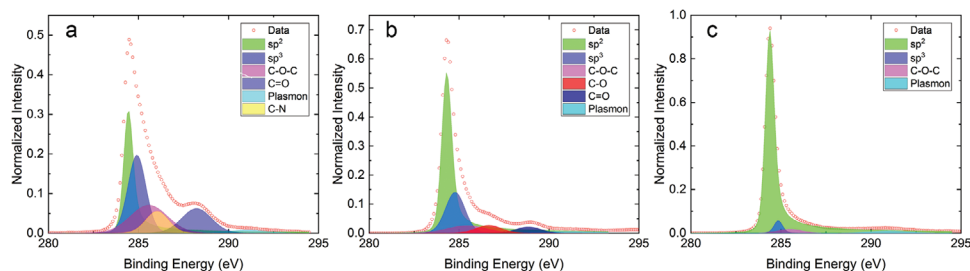FUNCTIONAL
MATERIALS
www.afm-journal.de

Figure 6. High-resolution C1s XPS spectra of graphene flakes in a) NMP, b) cyrene, and c) ethanol (after solvent exchange from cyrene). Additional data can be found in Table S2, Supporting Information.

from the cyrene solvent appears much lower after the solvent exchange to ethanol, that is, 4% instead of 19%. A carbon content of more than 95% after solvent exchange was observed, demonstrating that this processing step effectively removes cyrene residues.

C1s spectra show the typical asymmetric profiles of graphene materials. The C1s spectrum can be fitted into different components typical of graphite: a prominent peak at 284.4 eV for sp^2 carbon with the corresponding satellite peak due to π–π* (HOMO-LUMO) transition at 290.8 eV; a second peak around 285.0 eV related to sp^3-hybridized carbon, typically due to the flake edges and defects. The sp^3 fraction reduces from ≈25% to ≈5% (**Table 2**) after the solvent exchange process, indicating that part of the sp^3 carbons peak could be attributed to the presence of cyrene, before the solvent exchange procedure.

All the samples mainly show the presence of carbon weakly bonded to oxygen (apart for small C=O components), most likely due to solvent residues on the substrate and the surface of the graphene flakes. Finally, a remarkable C−N component is found, consistently, in NMP.

3.2. Graphene-Based Touch Sensor Electrodes

The selected graphene dispersions in NMP and cyrene (produced by SM+TS) were further processed via a solvent exchange approach to prepare the spray-coating compatible inks GNE and GCE, as described in Section 2.4.1. Two rectangular transparent electrodes (2 × 20 cm^2) were produced with each respective ink. **Table 3** presents the parameters and performance of the two electrodes. The electrodes have a thickness of ≈150 nm in both cases, as measured by profilometry. The GCE electrode has the best combination of electrical conductivity and transparency: 290 Ω $\square^{-1}$ and 78%. Such a performance is notable when considering that only green solvents (biodegradable cyrene and ethanol) were used to produce the GCE ink.

Flexibility is one of the most interesting feature theoretically granted by graphene, in view of the many possibilities this opens in technology. To this end, we tested the electrical performance of our graphene-based electrodes when subject to intense bending (**Figure 7**). A series of 20 parallel diamond shaped electrodes were spray-coated on a 100 µm-thick PET substrate.

The resistance measurements were collected before, during and after bending on a cylindrical surface with curvature radius r = 28 mm, as shown in Figure 7. The average resistance value over the 20 electrodes on the flat and bent substrate was 41.6 and 41.7 kΩ, respectively. Remarkably, the resistance values in each electrode were basically unchanged upon bending. The values kept also stable when recovering to a flat position. These results show that with a bending radius of 28 mm and that the electrodes suffered no damage and did not lower their performance when operated under considerable strain (ε = 0.18%).

3.3. Graphene-Based Touch Sensor Prototype

As aforementioned, we teamed up with DISPLAX S.A. to test the use of our "green" graphene-based ink in an industrial context. We developed a graphene-based, semi-transparent touch sensor featuring 20 reception electrodes and 20 transmission electrodes with sub-micron thickness (as described in Section 2.4.3 and Figure S3, Supporting Information). The touch screen sensor consisted of top and bottom spray-coated graphene sheets laminated together with a dielectric layer in between, forming a capacitive diamond-patterned flexible sensor stack (Figure S4, Supporting Information). The stack was finally laminated on a glass sheet to ease the test procedures. **Figure 8** illustrates the components and the final prototype under testing. The sensor was interfaced to a custom-made electronic controller and operated as a touch screen, having the detected touch input signal reported to a computer after analog-to-digital conversion.

Table 2. XPS peak percentage weights as determined from the spectra in Figure 6.

	sp^2	sp^3	C−O−C	C−N	C−O	C=O
NMP	27.0%	28.1%	20.4%	10.1%	0.0%	14.5%
Pre-cyrene	56.3%	24.8%	9.2%	0.0%	6.4%	3.3%
Post-cyrene (after solvent exchange)	91.1%	4.9%	4.0%	0.0%	0.0%	0.0%

**ADVANCED
SCIENCE NEWS**

www.advancedsciencenews.com

**ADVANCED
FUNCTIONAL
MATERIALS**

www.afm-journal.de

Table 3. Spray-coated, transparent, conductive electrodes on PET substrate made with GNE and GCE inks. The fabrication was done at room temperature with no post-annealing treatments.

Ink	Original solvent	Final solvent	Fabrication of the graphene electrode: Condition and parameters				
			Drying temperature [°C]	Drying time [min]	Thickness [nm]	Sheet resistance [$\Omega\ \Box^{-1}$]	Transmittance [%]
GNE	NMP	ethanol	25	10	150	370	65
GCE	cyrene	ethanol	25	10	150	290	78

The GCE ink was used to fabricate the final electrodes to be used in the touch sensor prototype.

The prototype was characterized in terms of industry-relevant parameters for touch-sensors and displays. As a first remark, the electrode thickness of ≈150 nm is well below the maximum trace height of 5 µm required by display manufacturers. Electrical resistance measurements were performed on the vertical and horizontal graphene electrodes—transmission (T_x) and reception (R_x). The electrode resistance is a critical parameter for this kind of device because it largely determines the signal attenuation and the overall sensor performance. The electrode resistance showed to be constant throughout the sensor: the average value is 30 kΩ for the rows, and 9.7 kΩ for the columns (Table S3, Supporting Information). The optical transmittance of the rows layer and columns layer is 78% and 75%, respectively. The sensor's overall transmittance, with laminated row, column, and dielectric layers, was 65.3%. High and low storage temperature, operation temperature, and humidity were also assessed. To that end, the touch-sensors were tested before and after storing at low (≈5 °C) and high temperatures (≈60 °C). During these tests, no degradation of touch detection was observed, nor any structural damage. The sensor's performance at different temperatures was tested (i.e., immediately after heating in an oven at 60 °C, and after cooling to room temperature), indicating no changes in touch detection. The sensor was also tested for operation in humid ambient atmospheres from 20% to 100% humidity, without noticeable

behavior change, and spraying it with water droplets produced no performance loss.

Analog signals, resulting from accumulated charge at the nodes (see Figures S4, Supporting Information), were acquired from every row-column node. The signal to noise ratio (SNR) defined as:

$$SNR\ (dB) = 10\log\left(\frac{V_{signal}}{V_{noise}}\right) \quad (2)$$

V_{signal} and V_{noise} are the signal and noise voltages measured in all the sensor nodes, showing a low and constant attenuation across the sensor area. The SNR is 14.0, 13.9, and 13.9 dB at nodes with coordinates 1 × 1, 10 × 10, and 20 × 20, located in different sensor regions (Figure 8c). This feature is of great importance for a high-sensitivity, marketable product. The high-sensitivity allowed our graphene prototype to be operated in a multi-touch mode (up to four simultaneous finger touches—three shown in the figure) with constant attenuation across the sensor area (**Figure 9**).

According to industrial display requirements, a commercially competitive touch sensor should feature an R_s of 50 Ω $\Box^{-1}$ with an optical transmittance of 86% at minimum (Table S4, Supporting Information). Comparing the results of our graphene-based prototype to these industrial requirements, it is apparent that further optimization of the current ratio of sheet resistance (290 Ω $\Box^{-1}$) and optical transmittance (78%) is required. As a prospective pathway toward better performance ratio, the spray-coated electrodes on PET could be hot-pressed to foster the interconnection between flakes in the film, thus reducing the sheet resistance while retaining approximately the same level of transparency. It should be noted, however, that our prototype relied on very thin electrodes (only 150 nm, well below the industrial requirement) and in turn showed remarkable results in mechanical flexibility that compete and surpass the industrial standard—withstanding a ~~high~~ bending radius without any change in functionality and performance. Besides, optical transparency is not a fixed requirement for touch surfaces (e.g., it is not necessary for drawing tablets[45] keyboards with touch surfaces,[46] and other touch-sensitive user interfaces[47]), and so our graphene-based inks could already find application in this kind of devices, possibly exploiting the flexibility they can confer to the fabricated components.

In the current market for touch sensors, the primary factor is the production cost, as the profit margins are becoming increasingly thin. For a sensor to be competitive, the production method should be cost-efficient: All the fabrication steps such as the materials preparation, deposition and patterning, as well as the curing processes of the sensor layers, should be
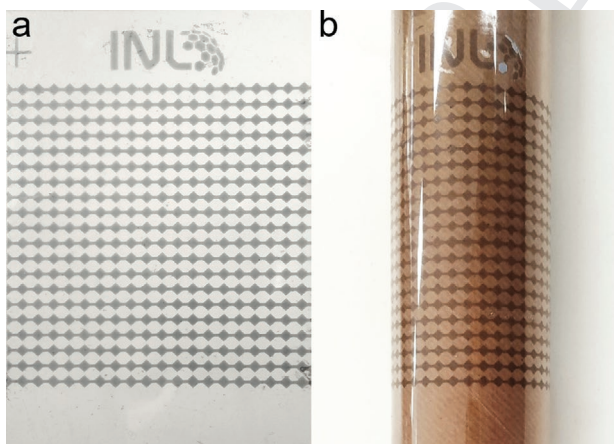

Figure 7. Graphene-based electrodes: a) before and b) after bending. The PET substrate was bent to the cylindrical surface shown in Figure 7, with a curvature radius of $r = 28$ mm. Disregarding the graphene electrode thickness (150 nm) compared with the PET substrate thickness, $t = 100$ µm, and assuming that the substrate's neutral plane is located in the middle of the PET sheet (which is reasonable since it is homogeneous with a constant thickness over the entire area), the strain induced in the bent graphene electrodes can be estimated as $\varepsilon = \frac{t}{2r} = 0.18\%$.
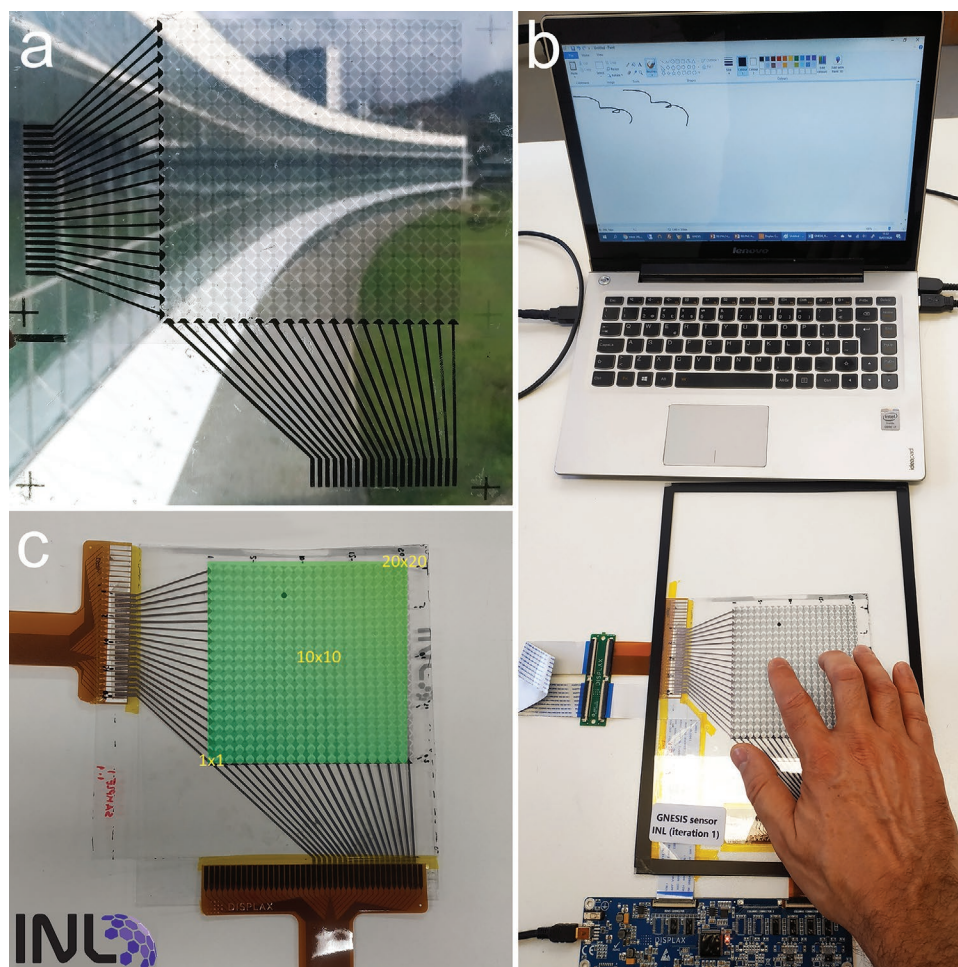
Figure 8. Graphene-based touch sensor prototype. a) Overlapped top and bottom PET panels with the spray-coated graphene row (T_x) and column (R_x) electrodes and conductive Ag pads. b) Complete system (touch sensor + controller + computer) operated in multi-touch mode. c) Complete touch sensor interfaced with external connections.

as simple as possible and realized with affordable equipment. In this context, material deposition techniques such as inkjet, screen printing, or spray coating—all suitable for GBMs—represent an optimal option for the sensor industry. Our results show that graphene is a viable option to answer the industry requests, as it can deliver suitable mechanical, visual, and electrical performance, while requiring simple and inexpensive deposition techniques. Overall, our green and cost-effective approach may find fruitful application in consumer and flexible electronics.

4. Conclusions

We proposed a strategy for a highly effective liquid-phase exfoliation of graphite to produce graphene-based
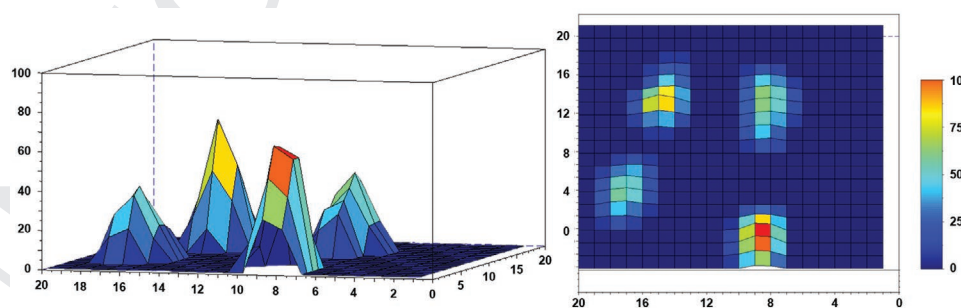

Figure 9. Touch peaks resulting from the graphene sensor operation with four fingers. Perspective-view on the left, matrix/frame top-view with color-coded peaks on the right. The vertical scale is in arbitrary units; the color code is the same in both figures.

**ADVANCED
SCIENCE NEWS**
www.advancedsciencenews.com

**ADVANCED
FUNCTIONAL
MATERIALS**
www.afm-journal.de

dispersions. Different methods as shear-mixing, tip-sonication, and the combination of the two processes in various solvents (NMP, DMF, and cyrene) were studied in detail to evaluate their impact on the graphene flake size, thickness, and overall concentration yield in the liquid dispersions. The "green" solvent—cyrene—was identified and studied in comparison to NMP and DMF, which are typical solvents for the LPE of graphite with known issues in terms of toxicity and substrate compatibility. Raman, TEM, and AFM were used to evaluate the crystalline quality and morphology of the graphene flakes in the various dispersions. The graphene flakes produced via shear-mixing demonstrated higher crystalline quality, and smaller lateral size and thickness than those obtained by tip-sonication. Remarkably, the combination of the two processes generated stable graphene flake dispersions with much higher concentration than the individual processes. The choice of solvent for the graphite exfoliation into few-layer graphene flakes is crucial for any foreseeable commercial production and application, and cyrene could thus pave the way for a scalable production. The inks produced with cyrene had the highest graphene flake concentration, smallest flake sizes, and a generally narrower flake size distribution. According to these results, cyrene can replace toxic and hazardous NMP and DMF solvents for this purpose.

We used our eco-friendly graphene ink to fabricate electrodes for a touch screen sensor prototype to demonstrate cyrene processing's viability for the fabrication of graphene-based technology. The challenge in the fabrication of transparent conductive electrodes pertains the balance among the three main characteristics: electrical performance, visual performance, and mechanical flexibility (high bending radius with unmodified performance). Our touch sensor prototype showed valuable performance across the board: optical transmittance of 78%, sheet resistance of 290 $\Omega \square^{-1}$, and no significant change in sheet resistance when bent to a curvature radius of 28 mm. Remarkably, given the low level of attenuation and high SNR, the sensor could be operated in multi-touch mode, with up to four simultaneous finger touches detected. Our results showed that LPE graphene from a "green solvent" could serve as the primary material for electrodes in flexible devices with high electrical performance, in compliance with the strain levels that a flexible device is expected to accommodate. Both the graphene-based ink formulation and the deposition techniques could easily tuned to maximize the electrical conductivity at the expense of the optical transparency, which is not a requirement for several consumer applications. Overall, the proposed LPE strategy approach can produce graphene-based dispersions with desired characteristics, low production cost (all processes occur at room temperature), and environmental compatibility, which can be excellent candidates for the fabrication of a wide range of electronic devices.

Supporting Information

Supporting Information is available from the Wiley Online Library or from the author.

Conflict of Interest

The authors declare no conflict of interest.

Data Availability Statement

Research data are not shared.

[1] K. S. Novoselov, A. K. Geim, S. V. Morozov, D. Jiang, Y. Zhang, S. V. Dubonos, I. V. Grigorieva, A. A. Firsov, *Science* **2004**, *306*, 666.

[2] K. S. Novoselov, V. I. Fal'Ko, L. Colombo, P. R. Gellert, M. G. Schwab, K. Kim, *Nature* **2012**, *490*, 192.

[3] M. Aliofkhazraei, N. Ali, W. I. Milne, C. S. Ozkan, S. Mitura, J. L. Gervasoni, in *Graphene Science Handbook Applications and Industrialization*, CRC Press, Boca Raton, FL **2016**.

[4] A. K. Geim, K. S. Novoselov, *Nat. Mater.* **2007**, *6*, 183.

[5] S. J. Kim, K. Choi, B. Lee, Y. Kim, B. H. Hong, *Annu. Rev. Mater. Res.* **2015**, *45*, 63.

[6] S. Das, P. Sudhagar, Y. S. Kang, W. G. Choi, *J. Mater. Res.* **2014**, *29*, 299.

[7] F. Bonaccorso, L. Colombo, G. Yu, M. Stoller, V. Tozzini, A. C. Ferrari, R. S. Ruoff, V. G. Pellegrini, *Science* **2015**, *347*, 1246501.

[8] S. Goenka, V. Sant, S. Sant, *J. Controlled Release* **2014**, *173*, 75.

[9] J. Santos, M. Moschetta, J. Rodrigues, P. Alpuim, A. Capasso, *Front. Bioeng. Biotechnol.* **2021**, *9*, 1.

[10] A. Capasso, J. Rodrigues, M. Moschetta, F. Buonocore, G. Faggio, G. Messina, M. J. Kim, J. Kwon, E. Placidi, F. Benfenati, M. Bramini, G. H. Lee, N. Lisi, *Adv. Funct. Mater.* **2020**, *31*, 2005300.

[11] A. Capasso, A. E. Del Rio Castillo, H. Sun, A. Ansaldo, V. Pellegrini, F. Bonaccorso, *Solid State Commun.* **2015**, *224*, 53.

[12] A. Capasso, S. Bellani, A. L. Palma, L. Najafi, A. E. Del Rio Castillo, N. Curreli, L. Cina, V. Miseikis, C. Coletti, G. Calogero, V. Pellegrini, A. Di Carlo, F. Bonaccorso, *2D Mater.* **2019**, *3*, 035007.

[13] K. Kostarelos, M. Vincent, C. Hebert, J. A. Garrido, *Adv. Mater.* **2017**, *29*, 1700909.

Q9

ADVANCED
SCIENCE NEWS
www.advancedsciencenews.com

ADVANCED
FUNCTIONAL
MATERIALS
www.afm-journal.de

[14] T. Reiss, K. Hjelt, A. C. Ferrari, *Nat. Nanotechnol* **2019**, *14*, 907.

[15] A. Elmarakbi, W. Azoti, *State of the Art on Graphene Lightweighting Nanocomposites for Automotive Applications*, Elsevier Inc., Amsterdam **2018**.

[16] A. G. Olabi, M. A. Abdelkareem, T. Wilberforce, E. T. Sayed, *Renewable Sustainable Energy Rev.* **2021**, *135*, 110026.

[17] D. S. Saidina, N. Eawwiboonthanakit, M. Mariatti, S. Fontana, C. Hérold, *J. Electron. Mater.* **2019**, *48*, 3428.

[18] M. Kim, J. H. Jeong, J.-Y. Lee, A. Capasso, F. Bonaccorso, S.-H. Kang, Y.-K. Lee, G.-H. Lee, *ACS Appl. Mater. Interfaces* **2019**, *11*, 11841.

[19] M. Segal, *Nat. Nanotechnol.* **2009**, *4*, 612.

[20] W. Kong, H. Kum, S.-H. Bae, J. Shim, H. Kim, L. Kong, Y. Meng, K. Wang, C. Kim, J. Kim, *Nat. Nanotechnol.* **2019**, *14*, 927.

[21] A. Narune, et al. *Graphene Market by Type (Mono-Layer & Bi-Layer Graphene, Few Layer Graphene, Graphene Oxide, and Graphene Nano Platelets), and Application (RFID, Composites, Sensors, Research & Development, Energy Storage, Functional Ink, and Polymer Additives), Tire, Coa* **2021**.

[22] Y. Lee, J. Kim, B. Jang, S. Kim, B. K. Sharma, J. H. Kim, J. H. Ahn, *Nano Energy* **2019**, *62*, 259.

[23] T. T. Huang, W. Wu, *Adv. Mater. Interfaces* **2020**, *7*, 1.

[24] F. Bonaccorso, A. Bartolotta, J. N. Coleman, C. Backes, *Adv. Mater.* **2016**, *28*, 6136.

[25] M. Kang, J. Kim, B. Jang, Y. Chae, J. H. Kim, J. H. Ahn, *ACS Nano* **2017**, *11*, 7950.

[26] F. Torrisi, T. G. Carey, *Nano Today* **2018**, *23*, 73.

[27] A. E. E. Del Rio Castillo, V. Pellegrini, A. Ansaldo, F. Ricciardella, H. Sun, L. Marasco, J. Buha, Z. Dang, L. Gagliani, E. Lago, N. Curreli, S. Gentiluomo, F. Palazon, M. Prato, R. Oropesa-Nunez, P. Toth, E. Mantero, M. Crugliano, A. Gamucci, A. Tomadin, M. Polini, F. Bonaccorso, *Mater. Horiz.* **2018**, *5*, 890.

[28] G. Faggio, G. Messina, C. Lofaro, N. Lisi, A. Capasso, *C* **2020**, *6*, 14.

[29] M. Gutiérrez, A. Henglein, *Ultrasonics* **1989**, *27*, 259.

[30] C. Backes, C. Berger, A. Beyer, R. Fasel, C. Merino, J. Mendez, H. Nolan, *2D Mater.* **2020**, 7.

[31] Y. Hernandez, V. Nicolosi, M. Lotya, F. M. Blighe, Z. Sun, S. De, I. T. McGovern, B. Holland, M. Byrne, Y. K. Gun'ko, J. J. Boland, P. Niraj, G. Duesberg, S. Krishnamurthy, R. Goodhue, J. Hutchison, V. Scardaci, A. C. Ferrari, J. N. Coleman, *Nat. Nanotechnol.* **2008**, *3*, 563.

[32] H. J. Salavagione, J. Sherwood, M. De Bruyn, V. L. Budarin, G. J. Ellis, J. H. Clark, P. S. Shuttleworth, *Green Chem.* **2017**, *19*, 2550.

[33] A. Amiri, M. Naraghi, G. Ahmadi, M. Soleymaniha, M. Shanbedi, *FlatChem* **2018**, *8*, 40.

[34] A. Jawaid, D. Nepal, K. Park, M. Jespersen, A. Qualley, P. Mirau, L. F. Drummy, R. A. Vaia, *Chem. Mater.* **2016**, *28*, 337.

[35] S. Majee, M. Song, S. L. Zhang, Z. B. Zhang, *Carbon* **2016**, *102*, 51.

[36] W. Zhao, M. Fang, F. Wu, H. Wu, L. Wang, G. Chen, *J. Mater. Chem.* **2010**, *20*, 5817.

[37] P. G. Karagiannidis, S. A. Hodge, L. Lombardi, F. Tomarchio, N. Decorde, S. Milana, I. Goykhman, Y. Su, S. V. Mesite, D. N. Johnstone, R. K. Leary, P. A. Midgley, N. M. Pugno, F. Torrisi, A. C. Ferrari, *ACS Nano* **2017**, *11*, 2742.

[38] K. R. Paton, E. Varrla, C. Backes, R. J. Smith, U. Khan, A. O'Neill, C. Boland, M. Lotya, O. M. Istrate, P. King, T. Higgins, S. Barwich, P. May, P. Puczkarski, I. Ahmed, M. Moebius, H. Pettersson, E. Long, J. Coelho, S. E. O'Brien, E. K. McGuire, B. M. Sanchez, G. S. Duesberg, N. McEvoy, T. J. Pennycook, C. Downing, A. Crossley, V. Nicolosi, J. N. Coleman, *Nat. Mater.* **2014**, *13*, 624.

[39] A. E. Del Rio Castillo, V. Pellegrini, A. Ansaldo, F. Ricciardella, H. Sun, L. Marasco, J. Buha, Z. Dang, L. Gagliani, E. Lago, N. Curreli, S. Gentiluomo, F. Palazon, M. Prato, R. Oropesa-Nuñez, P. S. Toth, E. Mantero, M. Crugliano, A. Gamucci, A. Tomadin, M. Polini, F. Bonaccorso, *Mater. Horiz.* **2018**, *5*, 890.

[40] M. Yi, Z. Shen, *J. Mater. Chem. A* **2015**, *3*, 11700.

[41] D. McManus, S. Vranic, F. Withers, V. Sanchez-Romaguera, M. Macucci, H. Yang, R. Sorrentino, K. Parvez, S. K. Son, G. Iannaccone, K. Kostarelos, G. Fiori, C. Casiraghi, *Nat. Nanotechnol.* **2017**, *12*, 343.

[42] Y. Arao, M. Kubouchi, *Carbon* **2015**, *95*, 802.

[43] R. Durge, R. V. Kshirsagar, P. Tambe, *Procedia Eng.* **2014**, *97*, 1457.

[44] K. Pan, Y. Fan, T. Leng, J. Li, Z. Xin, J. Zhang, L. Hao, J. Gallop, K. S. Novoselov, Z. Hu, *Nat. Commun.* **2018**, *9*, 5197.

[45] Wacom. Wacom Interactive pen displays, pen tablets and stylus products, https://www.wacom.com/en-us (accessed: March 2021).

[46] G. CK5, Cleankeys keyboard with a touch surface | washable-keyboards.com, https://www.washable-keyboards.com/portfolio-view/ck5-cleankeys-glass-keyboard-with-touch-surface/ (accessed: March 2021).

[47] Quad Industries. Manufacturing Printed Electronics | Membrane Switches | Haptic Touch, https://www.quad-ind.com/user-interfaces/capacitive-touch/ (accessed: March 2021).

[48] S. Kim, T. H. Phung, S. Kim, M. K. Rahman, K. S. Kwon, *Adv. Mater. Technol.* **2020**, *5*, 2000441.

[49] C. C. Wu, *Sol. Energy Mater. Sol. Cells* **2020**, *207*, 110350.

[50] H. Ling, R. Chen, Q. Huang, F. Shen, Y. Wang, X. T. Wang, *Green Chem.* **2020**, *22*, 3208.

[51] M. Hengge, K. Livanov, N. Zamoshchik, F. Hermerschmidt, E. J. W. List-Kratochvil, *Flex. Print. Electron.* **2021**, *6*, 015009.

[52] D. J. Kim, D. Y. Hwang, J. Y. Park, H. K. Kim, *J. Alloys Compd.* **2018**, *765*, 1090.

[53] D. Nečas, P. Klapetek, *Cent. Eur. J. Phys.* **2012**, *10*, 181.

[54] Y. Grosu, N. Udayashankar, O. Bondarchuk, L. González-Fernández, A. Faik, *Sol. Energy Mater. Sol. Cells* **2018**, *178*, 91.

[55] H. Sun, A. E. Del Rio Castillo, S. Monaco, A. Capasso, A. Ansaldo, M. Prato, D. A. Dinh, V. Pellegrini, B. Scrosati, L. Manna, F. Bonaccorso, *J. Mater. Chem. A* **2016**, *4*, 6886.

[56] S. Wang, Y. Zhang, N. Abidi, L. Cabrales, *Langmuir* **2009**, *25*, 11078.

[57] Y. J. Kim, H. Yoo, C. H. Lee, J. B. Park, H. Baek, M. Kim, G. C. Yi, *Adv. Mater.* **2012**, *24*, 5565.

[58] E. B. Secor, T. Z. Gao, A. E. Islam, R. Rao, S. G. Wallace, J. Zhu, K. W. Putz, B. Maruyama, M. C. Hersam, *Chem. Mater.* **2017**, *29*, 2332.

[59] A. C. Ferrari, J. C. Meyer, V. Scardaci, C. Casiraghi, M. Lazzeri, F. Mauri, S. Piscanec, D. Jiang, K. S. Novoselov, S. Roth, A. K. Geim, *Phys. Rev. Lett.* **2006**, *97*, 187401.

[60] I. Childres, L. A. Jauregui, W. Park, H. Caoa, Y. P. Chena, *New Dev. Photon Mater. Res.* **2013**, 403.

[61] A. C. Ferrari, D. M. Basko, *Nat. Nanotechnol.* **2013**, *8*, 235.

[62] H. Wang, Y. Wang, X. Cao, G. Lan, *J. Raman Spectrosc.* **2009**, *40*, 1791.

[63] J.-B. Wu, M.-L. Lin, X. Cong, H.-N. Liu, P.-H. Tan, *Chem. Soc. Rev.* **2018**, *47*, 1822.

[64] M. Wall, *Thermo Sci* **2011**, 5.

[65] M. C. Prado, R. Nascimento, L. G. Moura, M. J. S. Matos, M. S. C. Mazzoni, L. G. Cancado, H. Chacham, B. R. A. Neves, *ACS Nano* **2011**, *5*, 394.

[66] R. Beams, L. G. Cançado, A. Jorio, A. N. Vamivakas, L. Novotny, *Nanotechnology* **2015**, *26*, 1.

[67] A. Jorio, E. H. Martins Ferreira, L. G. Cançado, C. A. Achete, R. B. Capaz, in *Physics and Applications of Graphene – Experiments*, IntechOpen, UK **2011**.

[68] A. Gnisci, G. Faggio, G. Messina, J. Kwon, J.-Y. Lee, G.-H. Lee, T. Dikonimos, N. Lisi, A. Capasso, *J. Phys. Chem. C* **2018**, *122*, 28830.

[69] L. M. Malard, M. A. Pimenta, G. Dresselhaus, M. S. Dresselhaus, *Phys. Rep.* **2009**, *473*, 51.

[70] A. Capasso, T. Dikonimos, F. Sarto, A. Tamburrano, G. De Bellis, M. S. Sarto, G. Faggio, A. Malara, G. Messina, N. Lisi, *Beilstein J. Nanotechnol.* **2015**, *6*, 2028.

[71] V. T. Nguyen, H. D. Le, V. C. Nguyen, T. T. T. Ngo, D. Q. Le, X. N. Nguyen, N. M. Phan, *Adv. Nat. Sci. Nanosci. Nanotechnol.* **2013**, *4*, 035012.

[72] A. Das, S. Pisana, B. Chakraborty, S. Piscanec, S. K. Saha, U. V. Waghmare, K. S. Novoselov, H. R. Krishnamurthy, A. K. Geim, A. C. Ferrari, A. K. Sood, *Nat. Nanotechnol.* **2008**, *3*, 210.

[73] J. S. Park, A. Reina, R. Saito, J. Kong, G. Dresselhaus, M. S. Dresselhaus, *Carbon* **2009**, *47*, 1303.

[74] V. N. Popov, *J. Phys.: Conf. Ser.* **2016**, *682*, 012013.

[75] A. C. R. Ferrari, *Solid State Commun.* **2007**, *143*, 47.

[76] C. Casiraghi, A. Hartschuh, H. Qian, S. Pliscanec, C. Georgia, A. Fasoli, K. S. Novoselov, D. M. Basko, A. C. Ferrari, *Nano Lett.* **2009**, *9*, 1433.

[77] A. C. Ferrari, J. Robertson, *Phys. Rev. B* **2000**, *61*, 14095.

[78] A. Eckmann, A. Felten, A. Mishchenko, L. Britnell, K. S. Novoselov, C. Casiraghi, *Nano Lett.* **2012**, *12*, 3925.

[79] C. Backes, K. R. Paton, D. Hanlon, S. Yuan, M. I. Katsnelson, J. Houston, R. J. Smith, D. McCloskey, J. F. Donegan, J. N. Coleman, *Nanoscale* **2016**, *8*, 4311.

[80] J. Hassoun, F. Bonaccorso, M. Agostini, M. Angelucci, M. G. Betti, R. Cingolani, M. Gemmi, C. Mariani, S. Panero, V. Pellegrini, B. Scrosati, *Nano Lett.* **2014**, *14*, 4901.

ADVANCED FUNCTIONAL MATERIALS

Reprint Order Form

Manuscript No.: _____

Customer No.: (if available) _____

Purchase Order No.: _____

Author: _____

Charges for Reprints in Euro (excl. VAT), prices are subject to change. Minimum order 50 copies; single issues for authors at a reduced price.

No. of pages	50 copies	100 copies	150 copies	200 copies	300 copies	500 copies
1– 4	345,—	395,—	425,—	445,—	548,—	752,—
5– 8	490,—	573,—	608,—	636,—	784,—	1077,—
9–12	640,—	739,—	786,—	824,—	1016,—	1396,—
13–16	780,—	900,—	958,—	1004,—	1237,—	1701,—
17–20	930,—	1070,—	1138,—	1196,—	1489,—	2022,—
every additional 4 pages	147,—	169,—	175,—	188,—	231,—	315,—

Information regarding VAT: The charges for publication of *cover pictures /reprints/issues/poster/Video abstracts/* are considered to be "supply of services" and therefore subject to German VAT. However, if you are an institutional customer outside Germany, the tax can be waived if you provide us with the valid VAT number of your company. Non-EU customers may have a VAT number starting with "EU" instead of their country code, if they are registered with the EU tax authorities. If you do not have a valid EU VAT number and you are a taxable person doing business in a non-EU country, please provide a certification from your local tax authorities confirming that you are a taxable person under local tax law. Please note that the certification must confirm that you are a taxable person and are conducting an economic activity in your country. **Note:** certifications confirming that you are a tax-exempt legal body (non-profit organization, public body, school, political party, etc.) in your country do not exempt you from paying German VAT.

Please send me send bill me for

☐ no. of reprints

☐ no. of issue
(1 copy: 28 Euro)

☐ high-resolution PDF file (330 Euro excl. VAT)
E-mail address: _____

❖ Special Offer:

If you order 200 or more reprints you will get a PDF file for half price.

Please note: It is not permitted to present the PDF file on the internet or on company homepages.

Cover Posters (prices excl. VAT)
Posters of published covers are available in two sizes:
☐ DIN A2 42 x 60 cm / 17 x 24in (one copy: 39 Euro)

☐ DIN A1 60 x 84 cm / 24 x 33in (one copy: 49 Euro)

Postage for shipping (prices excl. VAT)
overseas   +25 Euro
within Europe +15 Euro

_____
Date, Signature

VAT number: _____

Mail reprints / copies of the issue to:
_____
_____
_____
_____
_____

Send bill to:
_____
_____
_____
_____

☐ **I will pay by bank transfer**

☐ **I will pay by credit card**

VISA, Mastercard and AMERICAN EXPRESS

For your security please use this link (Credit Card Token Generator) to create a secure code Credit Card Token and include this number in the form instead of the credit card data. Click here:
https://www.wiley-vch.de/editorial_production/index.php

CREDIT CARD TOKEN NUMBER

					V									

WILEY-VCH